# A Hybrid Method for Low Reynolds Number Flow Past an Asymmetric Cylindrical Body

*By Michèle S. Titcombe, Michael J. Ward[1] and Mary Catherine Kropinski[2]*

**Abstract**

Low Reynolds number fluid flow past a cylindrical body of arbitrary shape in an unbounded, two-dimensional domain is a singular perturbation problem involving an infinite logarithmic expansion in the small parameter $\varepsilon$, representing the Reynolds number. We apply a hybrid asymptotic-numerical method to compute the drag coefficient, $C_D$, and lift coefficient, $C_L$, to within all logarithmic terms. The hybrid method solution involves a matrix $\mathbf{M}$, depending only on the shape of the body, which we compute using a boundary integral method. We illustrate the hybrid method results on an elliptic object and on a more complicated profile.

## 1 Introduction

We consider two-dimensional, steady, incompressible, viscous fluid flow at low Reynolds number past one cylindrical body that is asymmetric with respect to the direction of the uniform free-stream. We apply a hybrid asymptotic-numerical method (the hybrid method) to calculate the lift and drag coefficients, that are correct to all logarithmic terms. This is an extension of the analysis of Kropinski, Ward & Keller [10], who applied the hybrid method to determine an asymptotic expression for the drag coefficient of a cylindrical body that is symmetric about the direction of the free-stream. We will refer to this as the symmetric case. Low Reynolds number fluid flow can model the locomotion of micro-organisms (see Lighthill [12]) with a Reynolds number in the range of $10^{-3}$ to 1. In measuring the force that the fluid exerts on the cylinder, the dimensionless lift and drag coefficients are of particular interest.

In terms of dimensional variables, the Navier-Stokes equations for the velocity $\mathbf{u} = (u_1, u_2)$ and pressure $p$ of the fluid flow are

$$(\mathbf{u} \cdot \nabla)\mathbf{u} = -\frac{1}{\rho}\nabla p + \nu\Delta\mathbf{u}, \tag{1.1a}$$

$$\nabla \cdot \mathbf{u} = 0, \tag{1.1b}$$

with boundary conditions $\mathbf{u} = 0$ on $\partial D$, the closed boundary of the body, and $\mathbf{u} \to (U_\infty, 0)$ as $|\mathbf{x}| \to \infty$. Here, $\mathbf{u}$ and $p$ are functions of the spatial variable, $\mathbf{x} = (x_1, x_2)$, $\rho$ is the density,

---

[1]Michèle S. Titcombe and Michael J. Ward, Department of Mathematics, University of British Columbia, Vancouver, B. C. Canada, V6T 1Z2

[2]Mary Catherine Kropinski, Department of Mathematics and Statistics, Simon Fraser University, Burnaby, B. C. Canada, V5A 1S6

$\nu$ is the kinematic viscosity of the fluid, and $U_\infty$ is the magnitude of the uniform free-stream velocity. After non-dimensionalizing, we identify the Reynolds number, $\mathrm{Re} = \mathrm{U}_\infty \mathrm{L}/\nu$, where $L$ is a characteristic length scale of the body.

This problem is a singular perturbation problem, in which the Reynolds number is the small perturbation parameter. The Stokes approximation to the Navier-Stokes equations, which neglects inertial forces, is valid in a local (inner) region, close to the body, and the Oseen approximation, a linearization of the Navier-Stokes equations, is valid in a global (outer) region, far from the body.

In 1957, Kaplun [8] and Proudman & Pearson [16] used the method of matched asymptotic expansions to resolve the Stokes paradox in two-dimensional, steady, viscous flow past a circular cylinder. Proudman & Pearson formulated the problem in terms of the dimensionless stream function, whereas Kaplun used velocity and pressure in his formulation. In their separate studies, each were able to determine analytically the first two terms in an asymptotic expansion for the drag coefficient and, with some difficulty, Kaplun was able to determine the third term. Also, Kaplun remarked on how to obtain the form of an expansion for a cylinder of arbitrary cross-sectional geometry. This is known as the equivalence principle of Kaplun, which asymptotically links the drag coefficients of cylinders of any cross-sectional shape, to within all logarithmic terms.

Twenty-five years later, Shintani, Umemura & Takano [17] applied the method of matched asymptotic expansions to determine the lift and drag coefficients of an elliptic cylinder in low Reynolds number fluid flow. They were able to obtain terms up to order $(\log \mathrm{Re})^{-2}$ in the inner expansion for the lift and drag forces acting on the cylinder. However, the truncated series for the drag and lift coefficients are only accurate for moderately small Reynolds number. Thus, further terms are necessary to provide reasonable accuracy for a wider range of low Reynolds numbers. For the special case of an elliptic cross-section, we will compare the leading-order form of our lift coefficient result to theirs.

Shortly thereafter, in 1986, Lee & Leal [11] numerically implemented the method of matched asymptotic expansions using velocity and pressure as variables in their study of low Reynolds number flow past cylinders of arbitrary cross-sectional shape. Like Shintani _et al._, they were able to determine expressions for the lift and drag force on the cylinders that were correct up to order $(\log \mathrm{Re})^{-2}$.

In extending the work of Kropinski _et al._ [10], we allow the cylinder cross-section to be asymmetric with respect to the free-stream and hence, the body could have a non-zero lift force. For one cylindrical body, of arbitrary cross-sectional shape $D_0$ and asymmetric with respect to the free-stream, we construct an asymptotic solution for the lift and drag coefficients in the limit of $\mathrm{Re} \to 0$. In the symmetric case, the solution involves a shape-dependent parameter, $d$. In the asymmetric case, which we are presenting in this paper, the solution involves a matrix, $\mathbf{M}$, that depends on the cross-sectional shape, $D_0$. Changing

the shape of the body in the hybrid method solution is very easy, since we only need to recompute the matrix, $\mathbf{M}$. Also, applying the hybrid method enables us to sum all the logarithmic terms appearing in the expansions for the lift and drag forces, resulting in an error that is $O(\mathrm{Re}^p)$ instead of $O((\log \mathrm{Re})^{-q})$ for some positive $p$ and $q$.

The dimensionless stream function, $\psi$, satisfies

$$v_1 = \frac{\partial \psi}{\partial y}, \qquad v_2 = -\frac{\partial \psi}{\partial x},$$

where $\mathbf{v} = (v_1, v_2)$ is the fluid velocity. As is well-known, in terms of polar coordinates with the origin at the centroid of the body, the stream function satisfies

$$\Delta^2 \psi + \varepsilon J_r(\psi, \Delta \psi) = 0, \qquad (r, \theta) \notin D_0, \tag{1.2a}$$

$$\psi = \frac{\partial \psi}{\partial n} = 0, \qquad (r, \theta) \in \partial D_0, \tag{1.2b}$$

$$\psi \sim r \sin \theta, \qquad r = (x_1^2 + x_2^2)^{1/2} \to \infty. \tag{1.2c}$$

Here, $\varepsilon \equiv \mathrm{Re} = U_\infty L / \nu \ll 1$ is the Reynolds number based on the length scale $L$ of the cylinder cross-section $D_0$, and $J_r$ is the Jacobian, $J_r(f, g) \equiv r^{-1}(f_r g_\theta - g_r f_\theta)$.

In Sections 2 and 3, we outline the standard singular perturbation analysis of (1.2) in the two regions of the solution domain; the "Stokes" (inner) and "Oseen" (outer) regions. Using the asymptotic structure that unfolds in the standard analysis, we apply the hybrid method to the original problem (1.2) in Section 4 and formulate a problem for the stream function that is asymptotically related to the original. We will solve this related problem numerically by extending the finite-difference code of Kropinski $et\ al.$ [10]. The solution of the related problem contains the entire infinite logarithmic expansion of the flow field and the force coefficients. In Section 5, we describe the numerical methods for solving the hybrid related problem, including the calculation of the body shape-dependent matrix $\mathbf{M}$ and necessary modifications to the symmetric case finite-difference code. Finally, in Section 6, we illustrate the hybrid method results for the lift and drag coefficients of various objects, and discuss possible extensions to this work.

## 2 Asymptotic Expansion in the Stokes Region

In the Stokes (inner) region where $r = O(1)$, the stream function satisfies (1.2a) with $\varepsilon = 0$ and (1.2b). We declare $r$ and $\psi$ to be the Stokes variables and expand the stream function in the form

$$\psi(r, \theta; \varepsilon) = \sum_{j=1}^{\infty} \nu^j(\varepsilon) \psi_j(r, \theta) + \cdots, \tag{2.1}$$

3

where $\nu(\varepsilon) \equiv -1/\log\varepsilon$. Substituting (2.1) into (1.2a)–(1.2b), we find that $\psi_j$ for $j = 1, 2, \ldots$ satisfies

$$\Delta^2\psi_j = 0, \qquad (r, \theta) \notin D_0, \tag{2.2a}$$

$$\psi_j = \frac{\partial\psi_j}{\partial n} = 0, \qquad (r, \theta) \in \partial D_0. \tag{2.2b}$$

The asymptotic form of $\psi_j$ as $r \to \infty$ involves linear combinations of $\{r^3, r\log r, r, r^{-1}\}\cos\theta$ and $\{r^3, r\log r, r, r^{-1}\}\sin\theta$. To match with the Oseen expansion, the $r^3$ terms must vanish. Thus, we can write the far-field form of $\psi_j$ as

$$\psi_j \sim \mathbf{a}_j \cdot [(r\log r\cos\theta, r\log r\sin\theta) + \mathbf{M}(r\cos\theta, r\sin\theta)] + \cdots, \tag{2.3}$$

as $r \to \infty$. The far-field form of the stream function $\psi_j$ is motivated by the section on viscous flow problems of Hsiao & MacCamy [6]. In (2.3), $\mathbf{a}_j = (a_{cj}, a_{sj})$, for $j \geq 1$, are constant vectors that are independent of the Reynolds number, $\varepsilon$. Also, $\mathbf{M}$ is a $2 \times 2$ matrix that depends on the cross-sectional shape of the body and on its orientation with respect to the free-stream. The matrix $\mathbf{M}$ is analogous to the body shape-dependent parameter $d$ of the symmetric case in [10].

Thus, the Stokes expansion has the far-field structure

$$\psi \sim \sum_{j=1}^{\infty} \nu^j(\varepsilon)\,\mathbf{a}_j \cdot [(r\log r\cos\theta, r\log r\sin\theta) + \mathbf{M}(r\cos\theta, r\sin\theta)], \tag{2.4}$$

as $r \to \infty$. We can also write the far-field structure of the Stokes expansion as

$$\psi \sim \sum_{j=1}^{\infty} \nu^j(\varepsilon)\,\mathbf{a}_j \cdot [\mathbf{y}\log|\mathbf{y}| + \mathbf{M}\mathbf{y}], \tag{2.5}$$

as $r = |\mathbf{y}| \to \infty$. Here, $\mathbf{y} = (r\cos\theta, r\sin\theta)$. We compare this to the symmetric case that Kropinski *et al.* [10] studied in which, due to the symmetry of the flow field, it was only necessary to include $\sin\theta$ terms in the stream function expansion.

# 3   Asymptotic Expansion in the Oseen Region

In the Oseen (outer) region of the solution domain, where $r = O(\varepsilon^{-1})$, we introduce new variables $\rho = \varepsilon r$, $\mathbf{x} = \varepsilon\mathbf{y} = (\rho\cos\theta, \rho\sin\theta)$ and $\Psi(\rho, \theta; \varepsilon) = \varepsilon\psi(\rho\varepsilon^{-1}, \theta; \varepsilon)$, and expand $\Psi$ as

$$\Psi(\rho, \theta; \varepsilon) = \rho\sin\theta + \sum_{j=1}^{\infty} \nu^j(\varepsilon)\Psi_j(\rho, \theta) + \cdots. \tag{3.1}$$

Again, $\nu \equiv -1/\log\varepsilon$.

4

Substituting (3.1) into (1.2a) and (1.2c) and matching $\Psi$ as $\rho \to 0$ to the far-field form of the Stokes expansion in (2.4), we find that $\mathbf{a}_1 = (0, 1)$ so that $\Psi_1$ satisfies

$$L_{os}\Psi_1 \equiv \Delta^2\Psi_1 + \left(\frac{\sin\theta}{\rho}\frac{\partial}{\partial\theta} - \cos\theta\frac{\partial}{\partial\rho}\right)\Delta\Psi_1 = 0, \qquad \rho > 0, \qquad (3.2a)$$

$$\Psi_1 \to 0, \qquad \rho \to \infty, \qquad (3.2b)$$

$$\Psi_1 \sim (\log\rho + m_{22} + a_{s2})\rho\sin\theta + (m_{21} + a_{c2})\rho\cos\theta, \qquad \rho \to 0. \qquad (3.2c)$$

We will elaborate later on the significance of the form of the first constant vector, $\mathbf{a}_1$. In (3.2a), $L_{os}$ is the linearized Oseen operator and $\Psi_1$ is the linearized Oseen solution. In (3.2c), $m_{ij}$ is the entry in row $i$ and column $j$ of the matrix $\mathbf{M}$. For $j = 2, 3, \ldots$, the functions $\Psi_j$ satisfy

$$L_{os}\Psi_j = -\sum_{k=1}^{j-1} J_\rho[\Psi_k, \Delta\Psi_{j-k}], \qquad \rho > 0, \qquad (3.3a)$$

$$\Psi_j \to 0, \qquad \rho \to \infty, \qquad (3.3b)$$

$$\Psi_j \sim \mathbf{a}_j \cdot [\mathbf{x}\log|\mathbf{x}| + \mathbf{M}\mathbf{x}] + \mathbf{a}_{j+1} \cdot \mathbf{x}, \qquad \rho = |\mathbf{x}| \to 0. \qquad (3.3c)$$

Again, the constant vectors $\mathbf{a}_j$ for $j = 2, 3, \ldots$ are independent of the Reynolds number, $\varepsilon$. The solution to (3.3) recursively determines these constant vectors.

For the symmetric body case, all the $a_{cj}$ components of $\mathbf{a}_j$ vanish. As well for this case, we show in Appendix B that the off-diagonal entries of the matrix $\mathbf{M}$ are zero.

For $\varepsilon \to 0$, the drag coefficient, $C_D$, and lift coefficient, $C_L$, for a cylinder of arbitrary cross-section are of the form (see Appendix A)

$$C_D \sim \frac{4\pi\nu}{\varepsilon}\left(\sum_{j=1}^{\infty} a_{sj}\nu^{j-1} + \cdots\right), \quad C_L \sim -\frac{4\pi\nu}{\varepsilon}\left(\sum_{j=2}^{\infty} a_{cj}\nu^{j-1} + \cdots\right). \qquad (3.4)$$

We begin the infinite sum in the lift coefficient expression at $j = 2$ since $a_{c1} = 0$ (recall that $\mathbf{a}_1 = (0, 1)$). At this stage, we see that with $\nu \equiv -1/\log\varepsilon$, where $\varepsilon$ is the Reynolds number, the coefficient of drag is $O((\varepsilon\log\varepsilon)^{-1})$ and the coefficient of lift is $O(\varepsilon^{-1}(\log\varepsilon)^{-2})$.

Kaplun's three-term expression for the drag coefficient provides a poor approximation of the experimental values unless $\varepsilon$ is very small (see Van Dyke [19]). Numerically, it is possible to compute further coefficients in the series from the infinite sequence of partial differential equations. However, one would still have to truncate the series at some finite $j$. Instead of truncating the series for the lift and drag coefficients, we show that the hybrid asymptotic-numerical method allows us to sum all the terms in the infinite logarithmic series while avoiding the direct and tedious calculations of the individual coefficients in the asymptotic expansions.

# 4 The Hybrid Method Formulation

We define the vector function $\mathbf{A}(\varepsilon)$ as asymptotic to the infinite logarithmic series

$$\mathbf{A}(\varepsilon) = (A_c(\varepsilon), A_s(\varepsilon)) \sim \sum_{j=1}^{\infty} \mathbf{a}_j \nu^{j-1}(\varepsilon), \qquad \varepsilon \to 0. \tag{4.1}$$

As in the previous section, the $\mathbf{a}_j = (a_{cj}, a_{sj})$ for $j \geq 1$ are constant vectors, and $\nu \equiv -1/\log \varepsilon$ where $\varepsilon$ is the Reynolds number. To obtain these constant vectors, it would be necessary to solve a recursive set of linearized, forced Oseen problems. In the symmetric case, Kaplun [8] was able to determine $a_{sj}$ for $j = 1, 2, 3$. However, it is analytically intractable to calculate any more of the $a_{sj}$. For this reason, we will apply the hybrid method in order to find $\mathbf{A}(\varepsilon)$ directly. We define the vector function $\boldsymbol{\psi}_c(\rho, \theta) = (\psi_c^x(r, \theta), \psi_c^y(r, \theta))$ to be the canonical inner solution satisfying

$$\Delta^2 \boldsymbol{\psi}_c = 0, \qquad (r, \theta) \notin D_0, \tag{4.2a}$$

$$\boldsymbol{\psi}_c = \frac{\partial \boldsymbol{\psi}_c}{\partial n} = 0, \qquad (r, \theta) \in \partial D_0, \tag{4.2b}$$

$$\boldsymbol{\psi}_c \sim \mathbf{y} \log |\mathbf{y}| + \mathbf{M}\mathbf{y}, \qquad r = |\mathbf{y}| \to \infty, \tag{4.2c}$$

where $\mathbf{M}$ is a 2x2 matrix that depends on the shape of the body. The solution of the canonical inner problem for a specific cylinder cross-section provides the matrix $\mathbf{M}$ for that shape. For certain cross-sectional shapes, such as an ellipse, it is possible to determine $\mathbf{M}$ analytically. In Appendix B, we show how to determine $\mathbf{M}$ for an ellipse inclined at an angle $\alpha$ to the free-stream. For a body of arbitrary shape, we provide a numerical method in Section 5.1 to find the $\mathbf{M}$ for that shape. The canonical problem in (4.2) is a vector analogue in terms of polar coordinates of the canonical local problem of the symmetric case.

Using (4.1) and (4.2) together with (2.3), the Stokes expansion (2.1) is asymptotic to

$$\psi(r, \theta; \varepsilon) = \nu(\varepsilon) \mathbf{A}(\varepsilon) \cdot \boldsymbol{\psi}_c(r, \theta) + \cdots . \tag{4.3}$$

Substituting (4.2c) into (4.3) and writing the result in terms of the Oseen variable $\mathbf{x} = \varepsilon \mathbf{y}$, we get the far-field form

$$\psi \sim \varepsilon^{-1} \mathbf{A}(\varepsilon) \cdot [\mathbf{x} + \nu(\varepsilon)\mathbf{x} \log |\mathbf{x}| + \nu(\varepsilon)\mathbf{M}\mathbf{x}], \qquad |\mathbf{y}| \to \infty. \tag{4.4}$$

We now formulate the related problem for the stream function. The related problem for $\mathbf{A}(\varepsilon)$ and the auxiliary stream function $\Psi_H \equiv \Psi_H(\rho, \theta; \varepsilon)$ is

$$\Delta^2 \Psi_H + J_\rho(\Psi_H, \Delta \Psi_H) = 0, \qquad \rho = |\mathbf{x}| > 0, \tag{4.5a}$$

$$\Psi_H \sim \rho \sin \theta, \qquad \rho \to \infty, \tag{4.5b}$$

$$\Psi_H \sim \mathbf{A}(\varepsilon) \cdot [\mathbf{x} + \nu(\varepsilon)\mathbf{x} \log |\mathbf{x}| + \nu(\varepsilon)\mathbf{M}\mathbf{x}], \qquad \rho \to 0. \tag{4.5c}$$

6

The solution to the related problem, using the method that we describe in Section 5.2, will allow us to compute $\mathbf{A}(\varepsilon)$.

The related problem is a hybrid asymptotic-numerical formulation of the original problem (1.2) but in terms of the Oseen (outer) variables. In the related problem, we have replaced the boundary conditions on the cylindrical body in (1.2b) by the singularity structure (4.5c). We derived the form of the singularity through the far-field structure of the logarithmic expansion in the Stokes region. Applying the hybrid method reduces the problem to computing the solution to the parameter-dependent problem (4.5) instead of computing the solutions to the infinite sequence of outer problems in (3.3). In terms of $\mathbf{A}$, the asymptotic formula for the lift and drag coefficients (see Appendix A), valid to within all logarithmic terms, is

$$(C_L, -C_D) = -\frac{4\pi}{\varepsilon}[\nu(\varepsilon)\mathbf{A}(\varepsilon) + \cdots], \quad \nu(\varepsilon) = -1/\log\varepsilon. \tag{4.6}$$

We found that $\mathbf{a}_1 = (0,1)$, which we substitute into (4.1) to see that $A_c = O(\nu)$ and that $A_s = O(1)$. Thus, we see that the lift coefficient is smaller than the drag coefficient by a factor of $O((\log\varepsilon)^{-1})$.

# 5  Numerical Methods

We now describe our numerical methods for calculating the shape-dependent matrix $\mathbf{M}$ and for solving the hybrid problem (4.5).

## 5.1  Calculation of the Shape-Dependent Matrix M

We seek the vector function $\boldsymbol{\psi}_c(r,\theta) = (\psi_c^x(r,\theta), \psi_c^y(r,\theta))$ which satisfies the canonical inner problem in (4.2). As we mentioned in the previous section, the solution of (4.2) for a specific cylinder cross-sectional shape provides the matrix $\mathbf{M}$ for that shape. In Appendix B, we discuss how to determine $\mathbf{M}$ analytically in the case of an ellipse. However, for an arbitrary cross-section, numerical methods must be employed.

For the symmetric case, Kropinski *et al.* [10] found the canonical inner solution by first conformally mapping $\partial D_0$ to the unit disk and then solving the mapped equations in the interior of the disc using a finite-difference scheme. There are a number of limitations to this approach. First, a conformal mapping must be found, and while one exists in theory, it is often difficult and time-consuming to determine this mapping in practice. Second, the numerical method is only second-order accurate and third, it is computationally expensive. It is much more natural to formulate $\psi_c^x(r,\theta)$ and $\psi_c^y(r,\theta)$ as solutions to integral equations, and this is the approach we take here. This has the two-fold advantage that the numerical solution requires only a boundary and not a volume discretization and that the far-field behaviour given by (4.2c) is captured analytically by the kernels of the integral operator.

7

In this work, we employ the integral equation methods from Greengard, Kropinski & Mayo [4] for solving problems in Stokes flow. These methods are computationally robust, spectrally accurate and extremely efficient and we outline here the relevant details from this paper. Following the discussion of Mikhlin and others [13, 14, 15], we note that $W = \psi_c^x(r, \theta)$ or $\psi_c^y(r, \theta)$ can be expressed by Goursat's formula as

$$W(x, y) = \mathrm{Re}(\overline{z}\phi(z) + \chi(z)),$$

where $\phi$ and $\chi$ are analytic functions of the complex variable $z = re^{i\theta}$, and $\mathrm{Re}(f)$ denotes the real part of the complex-valued function $f$. The functions $\phi(z)$ and $\chi(z)$ are known as Goursat functions. A simple calculation leads to Muskhelishvili's formula

$$\frac{\partial W}{\partial x} + i\frac{\partial W}{\partial y} = \phi(z) + z\overline{\phi'(z)} + \overline{\chi'(z)}, \tag{5.1}$$

which provides an expression for the velocity field. Muskhelishvili's formula reduces the canonical inner problem to a problem in analytic function theory, namely that of finding $\phi$ and $\chi'(z)$ which satisfy zero velocity on the boundary $\partial D_0$ and have the asymptotic far-field behaviour given by (4.2c) as $|z| \to \infty$.

As in [4], the construction of functions $\phi$ and $\chi'$ are

$$
\begin{aligned}
\phi(z) &= \frac{1}{2\pi i}\int_{\partial D_0}\frac{\omega(\xi)}{\xi - z}\,d\xi + \int_{\partial D_0}\omega(\xi)ds + C\log z, \\
\chi'(z) &= \frac{1}{2\pi i}\int_{\partial D_0}\frac{\overline{\omega}(\xi)\,d\xi + \omega(\xi)\,d\overline{\xi}}{\xi - z} - \frac{1}{2\pi i}\int_{\partial D_0}\frac{\overline{\xi}\omega(\xi)}{(\xi - z)^2}\,d\xi + \frac{b}{z} + \overline{C}\log(z).
\end{aligned}
\tag{5.2}
$$

In the preceding expressions, $\omega(\xi)$ is an unknown density, $b$ is a real constant determined by

$$b = i\int_{\partial D_0}\omega(t)d\overline{t} - \overline{w}(t)dt.$$

and $C$ is a complex constant which, as we discuss below, is fixed by the nature of the far-field flow.

If we let $z$ tend to a point $t$ on the contour $\partial D_0$ and use the classical formulae for the limiting values of Cauchy-type integrals, we obtain from (5.1) and the boundary condition (4.2b) the Sherman-Lauricella integral equation

$$
\begin{aligned}
\omega(t) + \int_{\partial D_0}\omega(\xi)ds &+ \frac{1}{2\pi i}\int_{\partial D_0}\omega(\xi)\,d\left(\ln\frac{\xi - t}{\overline{\xi} - \overline{t}}\right) \\
&- \frac{1}{2\pi i}\int_{\partial D_0}\overline{\omega}(\xi)\,d\left(\frac{\xi - t}{\overline{\xi} - \overline{t}}\right) + \frac{\overline{b}}{t} = -2C\log|t| - \overline{C}\frac{t}{\overline{t}}.
\end{aligned}
\tag{5.3}
$$

We solve (5.3) numerically, using a Nyström discretization based on the trapezoidal rule. The resulting linear system is solved iteratively using GMRES coupled with the Fast Multipole Method (FMM) (see [1, 3, 5]) to compute matrix-vector products. The method has

| $N$ | # GMRES Iterations | CPU Time | Error |
|---|---|---|---|
| 256 | 29 | 6.2 | $0.50 \, 10^{0}$ |
| 512 | 30 | 12.5 | $0.25 \, 10^{-1}$ |
| 1024 | 30 | 27.6 | $0.12 \, 10^{-7}$ |
| 2048 | 30 | 74.1 | $0.30 \, 10^{-14}$ |

Table 1: Error in computed $\mathbf{M}$ values for $a = 1$, $b = 1/10$, $\alpha = -\pi/3$. The exact values are $m_{11} = .3023824553010749$, $m_{12} = m_{21} = -.3542831197299977$, $m_{22} = -.1067084537898340$.

super-algebraic convergence and the computational expense is $O(N)$, where $N$ is the number of discretization points on $\partial D_0$. These are great savings compared with direct methods ($O(N^3)$), or iterative methods without FMM ($O(N^2)$). For a further discussion on the properties of the numerical methods, see [4].

To compute the entries to the matrix $\mathbf{M}$ for a particular $\partial D_0$, consider the expression for the far-field velocity as given by the representations for the Goursat functions. Substituting (5.2) into (5.1) and taking the limit as $|z| \to \infty$, we get the leading terms in the far field to be

$$\phi(z) + z\overline{\phi'(z)} + \overline{\chi'(z)} \sim 2C \log|z| + \frac{1}{2}\overline{C}\frac{z}{\overline{z}} + \int_{\partial D_0} \omega(\xi)ds.$$

Computing the gradients of $\psi_c^x$ and $\psi_c^y$ in (4.2c) and comparing to the above, we see that to determine $m_{11}$ and $m_{12}$, we first solve (5.3) with $C = 1/2$. The matrix entries, $m_{ij}$, are then determined from the solution $\omega(t)$ by the following

$$m_{11} = \text{Re}\left(\int_{\partial D_0} \omega(\xi)ds\right) - \frac{1}{2}, \qquad m_{12} = \text{Im}\left(\int_{\partial D_0} \omega(\xi)ds\right).$$

To find the remaining two entries, we solve (5.3) with $C = i/2$ and

$$m_{21} = \text{Re}\left(\int_{\partial D_0} \omega(\xi)ds\right), \qquad m_{22} = \text{Im}\left(\int_{\partial D_0} \omega(\xi)ds\right) - \frac{1}{2}.$$

Here, Re(f) and Im(f) represent the real and imaginary parts of the complex-valued function $f$.

As a test for the numerical procedure, we compute Stokes flow past an ellipse of ratio 10:1 with $\alpha = \pi/3$ and compare the numerically determined matrix entries to those derived in Appendix B. The results are shown in Table 1 and all timings reported are for a SPARC Ultra 1.

Next, we compute $\mathbf{M}$ for a profile for which there are no analytic formulae. The example profile is shown in Figure 1, together with contours of vorticity. The boundary is discretized with 2048 points and the computed matrix entries are

$$\mathbf{M} = \begin{bmatrix} -1.0019045557844 & 0.1550966443197 \\ 0.1550966443197 & -0.5484962829688 \end{bmatrix}. \tag{5.4}$$
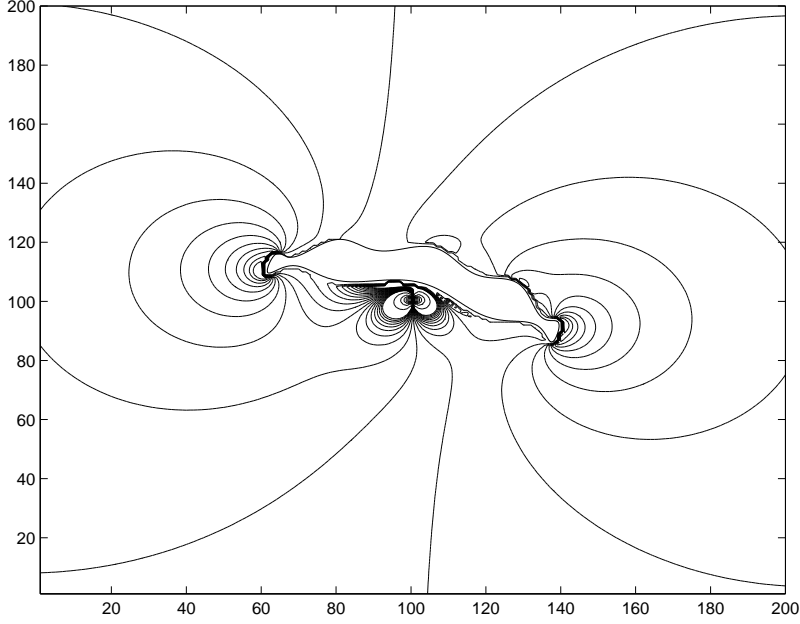
9

Figure 1: An example of the solution for a complicated profile $\partial D_0$. The plot shows contours of vorticity.

## 5.2 Numerical Solution of the Hybrid Method Related Problem

In numerically solving the parameter-dependent hybrid related problem in (4.5), we first decompose the solution as

$$\Psi_H(\rho, \theta; \varepsilon) = \rho \sin \theta + \nu(\varepsilon) \mathbf{A}(\varepsilon) \cdot (\Psi_{oc}, \Psi_{os}) + \Psi^*(\rho, \theta). \tag{5.5}$$

Using this expression, we will construct a problem to solve for $\Psi^*$ that is regular as $\rho \to 0$. In (5.5), $\Psi_{oc}$ and $\Psi_{os}$ correspond to the $\cos n\theta$ and $\sin n\theta$ parts of the linearized Oseen solution respectively. From the form of (3.2), we have that $\Psi_{oc}$ and $\Psi_{os}$ satisfy

$$L_{os}(\Psi_{oc}, \Psi_{os}) = \mathbf{0}, \qquad \rho > 0, \tag{5.6a}$$

$$(\Psi_{oc}, \Psi_{os}) \to \mathbf{0}, \qquad \rho \to \infty, \tag{5.6b}$$

$$\Psi_{oc} \sim \rho \log \rho \cos \theta, \quad \Psi_{os} \sim \rho \log \rho \sin \theta \qquad \rho \to 0. \tag{5.6c}$$

Here, $L_{os}$ is the linearized Oseen operator as defined in (3.2a).

The solution for $\Psi_{os}$, from Proudman & Pearson [16], is

$$\Psi_{os}(\rho, \theta) = -\sum_{n=1}^{\infty} \frac{\rho}{n} \left[ K_0\left(\frac{\rho}{2}\right) \left(I_{n-1}\left(\frac{\rho}{2}\right) + I_{n+1}\left(\frac{\rho}{2}\right)\right) + 2K_1\left(\frac{\rho}{2}\right) I_n\left(\frac{\rho}{2}\right) \right] \sin n\theta. \tag{5.7}$$

In this expression, $K_n(z)$ and $I_n(z)$ are modified Bessel functions of order $n$ of the first and second kind. In a similar manner (see Appendix C for details), we determine $\Psi_{oc}(\rho, \theta)$ to

10

be

$$\Psi_{oc}(\rho, \theta) = -4 \sum_{n=1}^{\infty} K_0\left(\frac{\rho}{2}\right) I_n\left(\frac{\rho}{2}\right) \cos n\theta. \tag{5.8}$$

For small $z = \rho/2$, the asymptotic forms as $z \to 0$ of the modified Bessel functions are

$$K_0(z) \sim -\log\left(\frac{z}{2}\right) - \gamma + \cdots, \quad K_1(z) \sim \frac{1}{z} + \cdots, \tag{5.9a}$$

$$I_0(z) \sim 1 + \cdots, \quad I_1(z) \sim \frac{z}{2} + \cdots. \tag{5.9b}$$

In (5.9a), $\gamma = 0.5772\ldots$ is Euler's constant. Using (5.9) in (5.7) and (5.8), we obtain that the asymptotic structures, as $\rho \to 0$, of $\Psi_{oc}$ and $\Psi_{os}$ are

$$\Psi_{oc} \sim \rho \log \rho \cos \theta + (\gamma - \log 4)\rho \cos \theta, \tag{5.10a}$$

$$\Psi_{os} \sim \rho \log \rho \sin \theta + (\gamma - \log 4 - 1)\rho \sin \theta, \qquad \rho \to 0. \tag{5.10b}$$

Substituting (5.5) into (4.5), and using (5.10), we have that $\Psi^*$ is regular as $\rho \to 0$ and satisfies

$$L_{os}\Psi^* = -J_\rho[\nu \mathbf{A} \cdot (\Psi_{oc}, \Psi_{os}) + \Psi^*, \nu \mathbf{A} \cdot (\Delta\Psi_{oc}, \Delta\Psi_{os}) + \Delta\Psi^*], \qquad \rho > 0, \tag{5.11a}$$

$$\Psi^* \to 0, \qquad \rho \to \infty, \tag{5.11b}$$

$$\Psi^* \sim [A_c + \nu(m_{11}A_c + m_{12}A_s - A_c(\gamma - \log 4))]\rho \cos \theta +$$

$$[A_s + \nu(m_{21}A_c + m_{22}A_s - A_s(\gamma - \log 4 - 1)) - 1]\rho \sin \theta + \cdots, \qquad \rho \to 0. \tag{5.11c}$$

Again, $\mathbf{A} = (A_c, A_s)$ and $m_{ij}$ is the $ij$th entry of the matrix $\mathbf{M}$. In Appendix C, we provide the linearized Oseen solution, $\Psi_{oc}$, and analytical formulae for its various derivatives that we require to evaluate numerically the Jacobian $J_\rho$ in (5.11a). The corresponding formulae for $\Psi_{os}$ are in the paper of Kropinski $et$ $al.$ [10] for the symmetric case.

We can also write (5.11c) in the form

$$\Psi^* = \Psi^{(c)}(\rho) \cos \theta + \Psi^{(s)}(\rho) \sin \theta + \cdots, \qquad \rho \to 0. \tag{5.12}$$

In (5.12), $\Psi^{(c)}$ and $\Psi^{(s)}$ are the Fourier cosine and sine coefficients respectively, given by

$$\Psi^{(c)} = \frac{1}{\pi} \int_0^{2\pi} \Psi^*(\rho, \theta) \cos \theta \, d\theta, \tag{5.13a}$$

$$\Psi^{(s)} = \frac{1}{\pi} \int_0^{2\pi} \Psi^*(\rho, \theta) \sin \theta \, d\theta. \tag{5.13b}$$

Here, $\Psi^{(c)}$ and $\Psi^{(s)}$ depend on $\rho \ll 1$ and on the vector parameter $\boldsymbol{\kappa} = (\kappa_c, \kappa_s) = \nu \mathbf{A}$.

We now outline the procedure to determine the vector $\mathbf{A}(\varepsilon)$, where $\varepsilon$ is the Reynolds number. Comparison of the two expressions for $\Psi^*$ as $\rho \to 0$ in (5.11c) and (5.12) results

in a $2 \times 2$ non-linear system for $\boldsymbol{\kappa}$ of the form

$$
\begin{bmatrix} m_{21} & \nu^{-1} + m_{22} - (\gamma - \log 4 - 1) \\ \nu^{-1} + m_{11} - (\gamma - \log 4) & m_{12} \end{bmatrix} \begin{bmatrix} \kappa_c \\ \kappa_s \end{bmatrix} = \begin{bmatrix} 1 + \lim_{\rho \to 0} \dfrac{\Psi^{(s)}(\kappa_c, \kappa_s)}{\rho} \\ \lim_{\rho \to 0} \dfrac{\Psi^{(c)}(\kappa_c, \kappa_s)}{\rho} \end{bmatrix}.
$$

$$(5.14)$$

For various $\boldsymbol{\kappa}$, we compute the solution $\Psi^*$ from the parameter-dependent problem (5.11a) and (5.11b), noting that $A_c = \nu^{-1} \kappa_c$ and $A_s = \nu^{-1} \kappa_s$. We fix $\rho = \delta \ll 1$ and using (5.13), we compute a "table of values" for the right-hand side of the non-linear system involving the Fourier sine and cosine coefficients. In the specific case of low Reynolds number fluid flow past an elliptic cylinder, we can find the $m_{ij}$ entries of the matrix $\mathbf{M}$ analytically (see Appendix B). For a general cross-sectional shape, we employ the numerical method of Section 5.1 to determine numerically the $m_{ij}$. For a given Reynolds number, $\varepsilon$, we have the value of $\nu \equiv -1/\log \varepsilon$. We can then solve the $2 \times 2$ non-linear system in (5.14) for $\boldsymbol{\kappa}(\varepsilon)$. We use a bi-cubic spline to interpolate values of the right-hand side of (5.14) at arbitrary $\boldsymbol{\kappa}$ from our "table of values" of the Fourier sine and cosine coefficients. To solve (5.14), we employ Newton's method in which we compute the Jacobian with centred finite differences. Finally, $\mathbf{A}(\varepsilon) = \nu^{-1} \boldsymbol{\kappa}(\varepsilon)$. With $\mathbf{A}(\varepsilon)$ in hand, we calculate the coefficients of lift and drag from the asymptotic expression in (4.6).

To compute the solution $\Psi^*$ from (5.11), we extend the finite difference code of Kropinski *et al.* [10]. They based their code for the symmetric case on a stream function/vorticity formulation of the problem and solved the resulting non-linear system of equations for the unknowns $\Psi^*(\rho, \theta)$ and $\omega^*(\rho, \theta) = \Delta \Psi^*(\rho, \theta)$ using Newton's iterations. They stretched the radial variable according to $\tau = \log(1 + \rho)$ and applied a second-order centred discretization on a uniform polar grid to the equations in terms of the variables $(\tau, \theta)$. Exploiting the symmetry of the flow field, they solved for the unknowns $\Psi^*$ and $\omega^*$ on the domain $0 < \tau \leq \tau_\infty, 0 \leq \theta \leq \pi$, where $\tau_\infty$ is an artificial far-field boundary.

The main modifications to the symmetric version of the code were: to expand the solution domain to $0 < \tau \leq \tau_\infty, 0 \leq \theta \leq 2\pi$ since the flow field is no longer symmetric in general; to determine the solution for various input vector parameters $\boldsymbol{\kappa} = (\kappa_c, \kappa_s)$ instead of the scalar parameter $\kappa$ in the symmetric case; and using a Fourier cosine and sine expansion to produce a $2 \times 2$ non-linear system to solve for the vector $\mathbf{A}(\varepsilon)$.

In the symmetric case, Kropinski *et al.* [10] could exploit the symmetry of the flow field to restrict the solution domain to the upper half plane. The corresponding computational domain was then $0 < \tau \leq \tau_\infty, 0 \leq \theta \leq \pi$. For flow past an arbitrarily shaped cylinder, the flow field is, in general, asymmetric. Thus, we extend the code to solve for $\Psi^*$ and $\omega^*$ on $0 < \tau \leq \tau_\infty, 0 \leq \theta \leq 2\pi$ and impose the periodicity conditions, $\Psi^*(\tau, 0) = \Psi^*(\tau, 2\pi)$ and $\omega^*(\tau, 0) = \omega^*(\tau, 2\pi)$. We enforce periodicity in the computations through the addition of an artificial grid line in the $\theta$-direction.

We add $\cos\theta$ terms to the linearized Oseen solution in the Jacobian term in (5.11a), which were not present in the symmetric case version of that equation, and compute the solution for various input vector parameters $\boldsymbol{\kappa} = (\kappa_c, \kappa_s)$ using $n$ values of $\kappa_c$ and $m$ values of $\kappa_s$. This is in contrast to the symmetric case where the parameter dependence was on a scalar $\kappa$, corresponding to our $\kappa_s$. For a given $\kappa_{c,i}$, for $i = 1, \ldots, n$, we compute $\Psi^*$ for a range of $\kappa_{s,j}$, for $j = 1, \ldots, m$, and at each stage, use the solution of the previous stage where $\boldsymbol{\kappa} = (\kappa_{c,i}, \kappa_{s,j-1})$ as the initial guess. When we step to the next value of $\kappa_c$, we use the solution from the stage where $\boldsymbol{\kappa} = (\kappa_{c,i}, \kappa_{s,1})$ as the initial guess for the stage where $\boldsymbol{\kappa} = (\kappa_{c,i+1}, \kappa_{s,1})$.

Kropinski *et al.* [10] matched the computed solution to its asymptotic structure near the origin in terms of its derivative, $\partial\Psi^*/\partial\tau$, which gave them a narrow range for the constants $A(\varepsilon)$. In contrast, we follow the technique in Keller & Ward [9] of comparing the form of the solution at the origin to an expansion in terms of its Fourier cosine and sine coefficients. This technique provides us with a $2 \times 2$ non-linear system to solve for $\boldsymbol{\kappa} = \nu\mathbf{A}$, and in turn, to find $\mathbf{A}$.

# 6    Results and Discussion

We present the results of our study through various examples using the cross-sectional shapes of an inclined ellipse and the profile in Figure 1. The shape of the cylinder cross-section enters into the hybrid method solution through the matrix $\mathbf{M}$, which we can determine analytically for an ellipse from (B.1). We use the numerical procedure of Section 5.2 to solve the hybrid related problem in (5.11) for the stream function $\Psi^*$ on a $100 \times 100$ grid with an artificial boundary condition corresponding to a radial variable of value $\rho_\infty = 60$. We use the solution for $\Psi^*$ to compute the Fourier sine and cosine coefficients in (5.13), which we require for solving the $2 \times 2$ non-linear system in (5.14) for $\mathbf{A}(\varepsilon) = \boldsymbol{\kappa}(\varepsilon)\nu^{-1}(\varepsilon)$. We then use $\mathbf{A}(\varepsilon)$ in (4.6) to obtain the coefficients of lift and drag, correct to all logarithmic terms.

## 6.1    An Elliptic Object

In examining the leading-order form of the asymptotic expansions for the lift and drag coefficients in (3.4), we find that the drag coefficient is $O(\nu/\varepsilon)$ and that the lift is $O(\nu^2/\varepsilon)$, where $\nu = -1/\log\varepsilon$. For an elliptic cylinder with major semi-axis $a$ and minor semi-axis $b$ inclined at an angle $\alpha$ to the free-stream at Reynolds number $\varepsilon$, the leading-order form of our expression for the lift coefficient, $C_L$, is

$$C_L = \frac{4\pi}{\varepsilon(\log\varepsilon)^2}\frac{a-b}{a+b}\sin\alpha\cos\alpha. \tag{6.1}$$

13

To obtain this leading-order form from (3.4), we need the first non-zero $a_c$-component of the constant vectors, $\mathbf{a}_j$. In Section 3, we found that the first constant vector is $\mathbf{a}_1 = (0, 1)$. We continue the matching procedure between the Stokes and Oseen regions to determine that the component $a_{c2}$ of the second constant vector, $\mathbf{a}_2$, is $a_{c2} = -m_{21}$, where $m_{21}$ is an entry of the body shape-dependent matrix $\mathbf{M}$. Substituting the matrix $\mathbf{M}$ for an inclined ellipse in (B.1) and the form of $a_{c2}$ into (3.4), we obtain our leading-order form for the lift coefficient of an inclined ellipse.
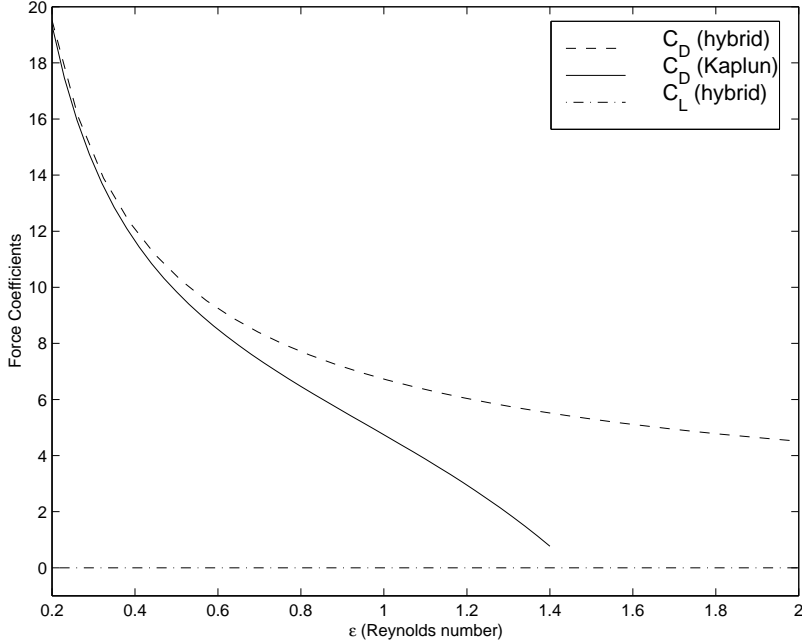


Figure 2: Drag coefficient, $C_D$ from the hybrid results and from Kaplun's three-term expansion, and the lift coefficient, $C_L$, from the hybrid results, versus Reynolds number, $\varepsilon$, of a circular cylinder (an ellipse with equal major and minor semi-axes $a = b = 1$).

We confirm the leading-order form of our result by comparing it with the leading-order expression for the lift coefficient of Shintani *et al.* [17] in their study of low Reynolds number flow past an elliptic cylinder. Their expression for the lift coefficient, correct to $O(\varepsilon^{-1}(\log \varepsilon)^{-2})$, can be written as

$$(C_L)_S \sim \frac{4\pi}{R(\log R - t_+)(\log R - t_-)} \left( \frac{a-b}{a+b} \right) \sin 2\alpha, \tag{6.2}$$

where

$$t_\pm = -\gamma + 4 \log(2) - \log[1 + b/a] \pm \frac{1}{2} \left\{ 1 + 2 \left( \frac{a-b}{a+b} \right) \cos 2\alpha + \left( \frac{a-b}{a+b} \right)^2 \right\}^{\frac{1}{2}}.$$

Here, $R = 2\varepsilon$ and $\gamma = 0.5772\ldots$ is Euler's constant. The leading-order expression of Shintani *et al.* [17] in (6.2) is consistent with our leading-order form in (6.1). In their

14

paper on flow past cylinders of arbitrary cross-sectional shape, Lee & Leal [11] numerically calculated the lift force, correct to $O((\log \varepsilon)^{-2})$, which corresponds to a lift coefficient of $O(\varepsilon^{-1}(\log \varepsilon)^{-2})$. They showed that their numerically calculated values for the lift agree with the analytical results of Shintani *et al.* [17] for an elliptic cross-section. Chester [2] examined the motion of an inclined elliptic cylinder at low Reynolds number and obtained an analytic expression for the lift force, correct to $O(\varepsilon^{-1}(\log \varepsilon)^{-2})$, that (once adjusted for the fluid in motion past a stationary body) is also consistent with our leading-order form. These results of previous researchers substantiate the form of the first term in our asymptotic expression for the lift coefficient as an infinite expansion of reciprocal logarithms. With the numerical solution of the hybrid related problem that we show in the following examples, we obtain the lift coefficient correct to all logarithmic terms.
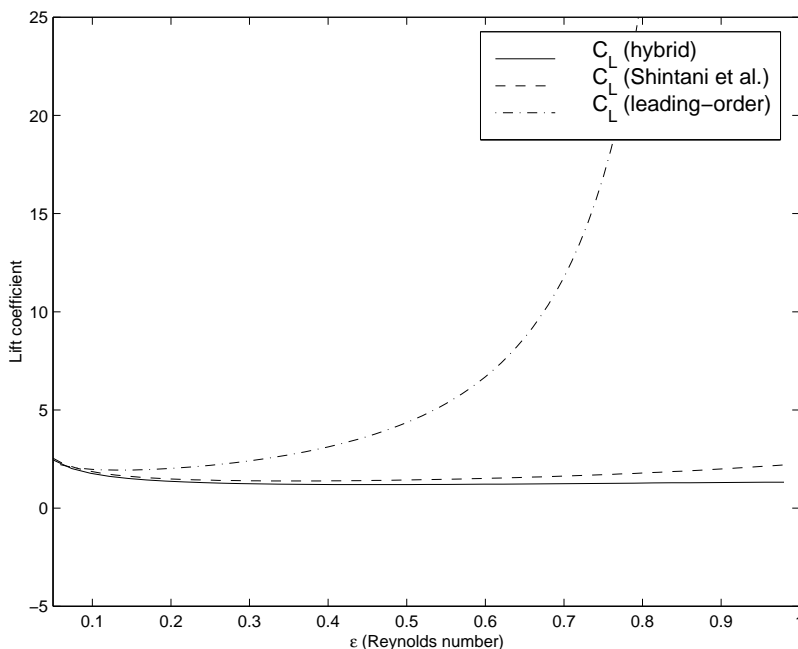


Figure 3: Lift coefficient, $C_L$, versus Reynolds number, $\varepsilon$, of an elliptic cylinder with major semi-axis $a = 1$ and minor semi-axis $b = 0.5$ at an angle of inclination, $\alpha = \pi/4$, comparing the hybrid results with the leading-order form in (6.1) and the results from Shintani *et al.* in (6.2).

**Varying the Reynolds Number.** First, we use the curve for the coefficient of drag as a check of the extended asymmetric code, to ensure that we compute the same solution as the original symmetric code of Kropinski *et al.* [10]. For a circular cross-section of radius 1 (an ellipse with equal major and minor semi-axes, $a = b = 1$), Figure 2 displays the force coefficients versus the Reynolds number, $\varepsilon$, showing a constant zero lift coefficient and the same coefficient of drag curve as produced in Kropinski *et al.* [10]. For the drag coefficient curve in Figure 2, we compare with the three-term expansion of Kaplun [8], which we can

write as

$$(C_D)_K \sim 4\pi\hat{\nu}[1 - 0.8669\hat{\nu}^2], \qquad \hat{\nu} \equiv \frac{1}{\log 3.7027 - \log \varepsilon}. \tag{6.3}$$

In Figure 3, we plot the lift coefficient versus Reynolds number, $\varepsilon$, for an elliptic cross-section with major semi-axis $a = 1$ and minor semi-axis $b = 0.5$ and at an angle of inclination of $\alpha = \pi/4$. The figure contains the $C_L(\varepsilon)$ curves from the hybrid method result correct to all logarithmic terms in (4.6), from the leading-order expression in (6.1), and from the result of Shintani *et al.* in (6.2). The plot shows reasonable agreement with the result of Shintani *et al.* [17], which is valid up to $O(\nu^2/\varepsilon)$. Figures 2 and 3 indicate that the three-term expansion for $C_D$ in (6.3) and the leading-order expression for $C_L$ in (6.1) are valid only for a narrow range of $\varepsilon$. Although the coefficient of lift from Shintani *et al.* is close to ours, their result is only for an elliptic object. In Section 6.2, we show the hybrid method results for the force coefficients on a more complicated object.
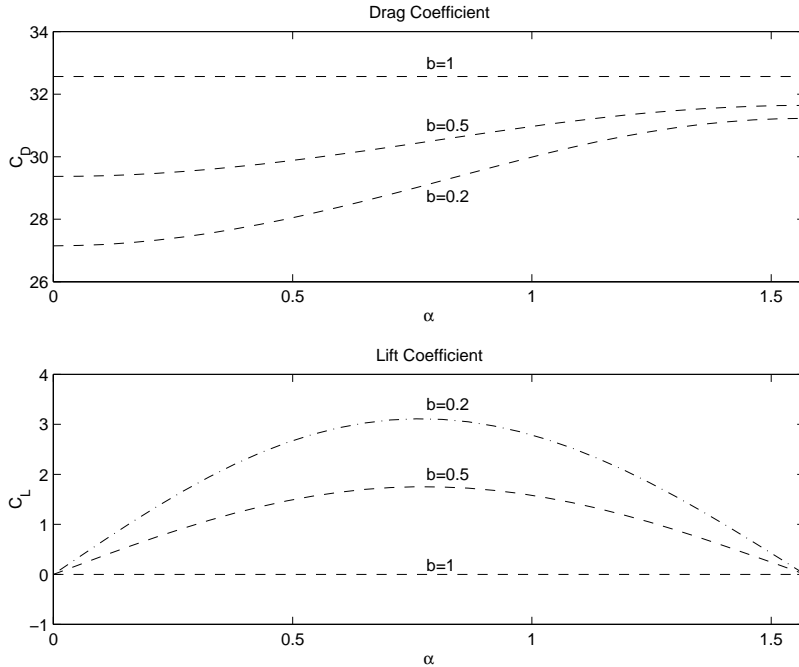


Figure 4: Lift coefficient, $C_L$, and drag coefficient, $C_D$, versus angle of incline, $\alpha$, of an elliptic cylinder with major semi-axis $a = 1$ and minor semi-axis $b = \{1.0, 0.5, 0.2\}$ at Reynolds number $\varepsilon = 0.1$.

**Varying the Angle of Incline.** In Figure 4, we fix the Reynolds number, $\varepsilon = 0.1$, and vary the angle of incline, $\alpha$, of the elliptic cylinder with major semi-axis $a = 1$ and minor semi-axis $b = 1, 0.5, 0.2$. In all cases, we see that at $\alpha = 0$ and $\alpha = \pi/2$, when the ellipse is symmetric to the free-stream, the coefficient of lift is 0. For the case with minor semi-axis $b = 1$, the cross-sectional shape is a circle, and as we expect, we see that the drag coefficient is constant and non-zero, and that the lift coefficient is 0. The figure also displays that

the drag coefficient increases as the angle of incline increases, and decreases as the minor semi-axis $b$ decreases.

The graphs in Figure 4 are qualitatively similar in nature to those of Lee & Leal [11], in which they plotted the contributions to the force on an elliptic cylinder at $O((1/\log \varepsilon)^2)$, where $\varepsilon$ is the Reynolds number, as a function of the angle of inclination, $\alpha$.

## 6.2   A More Complicated Object

We now demonstrate the hybrid method results on a more complicated object, whose profile is in Figure 5. Here, we need only modify the matrix $\mathbf{M}$, that depends on the body cross-sectional shape, to compute the force coefficients, $C_D$ and $C_L$.
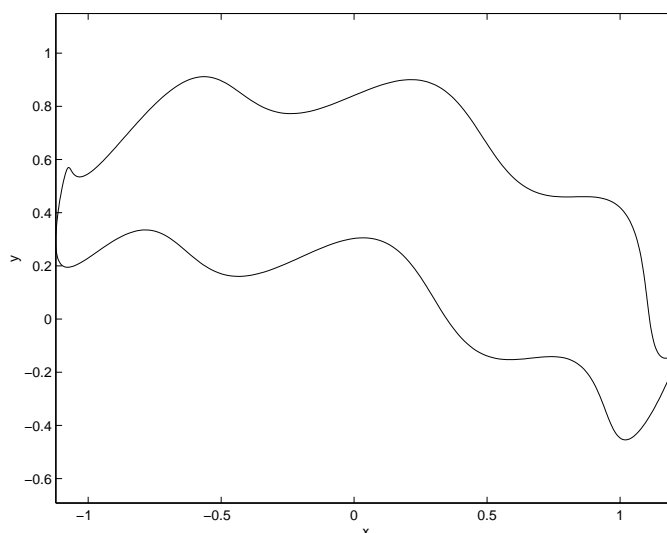


Figure 5: A more complicated object, whose profile is given by the analytical expression in (6.4).

**Varying the Reynolds Number.** In Figure 6, we plot the force coefficients versus Reynolds number, $\varepsilon$, for an object with a complicated cross-section. An analytical expression for a point $(x, y)$ on the boundary of this object is

$$x = \xi \cos \beta - \eta \sin \beta, \qquad y = \xi \sin \beta + \eta \cos \beta, \tag{6.4a}$$

where

$$\xi = \frac{a \cos \theta + a \cos \theta}{(a \cos \theta)^2 + (b + a \sin \theta)^2}, \quad \eta = \frac{b + a \sin \theta - (b + a \sin \theta)}{(a \cos \theta)^2 + (b + a \sin \theta)^2} + \frac{b}{3} \cos(N\theta), \tag{6.4b}$$

and

$$\beta = -0.3, a = 1.2, b = 0.3, N = 8, 0 \le \theta < 2\pi. \tag{6.4c}$$

To compute the matrix $\mathbf{M}$ for this complicated object, we employed the numerical method of Section 5.1 and obtained the matrix entries in (5.4).
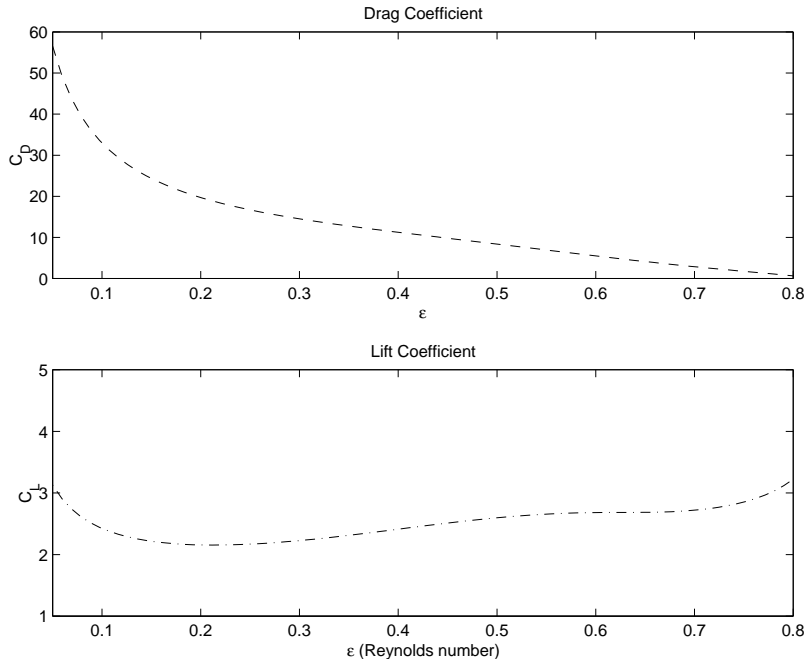
Figure 6: Drag coefficient, $C_D$, and lift coefficient, $C_L$, versus Reynolds number, $\varepsilon$, of a more complicated object, whose profile we show in Figure 5.

## 6.3   Possible Extensions

One possible extension to this work is to consider low Reynolds number fluid flow past an array of $N$ cylindrical bodies. In this case, we assume that the cross-sectional shapes are arbitrary with respect to the free-stream and construct asymptotic expressions for the drag coefficient of each body. The governing equations are the steady-state Navier-Stokes equations in (1.1). For this case involving multiple bodies, we would be able to examine the effect of the interaction between the bodies.

Two different limits in terms of the Stokes variables that we may consider are: a "lumped-body" limit where the bodies of $O(1)$ radii are separated by $O(1)$ distances, and an "unlumped-body" limit in which the radii of the bodies have magnitude of $O(1)$ and are separated by distances of $O(1/\varepsilon)$ where $\varepsilon \ll 1$ is the Reynolds number.

In the first limit, we can lump the bodies together via one matrix $\mathbf{M}$ for the entire array of cylinders and in such a way, reduce the problem to one considered above. The hybrid method would allow us to sum all of the logarithmic terms in the determination of the flow field. The lumped-body problem is analogous to the one-body problem in that one can consider the Stokes region containing all of the bodies. This was the approach of Lee & Leal [11] who used boundary integral methods to solve for low Reynolds number flow past multiple cylinders, assuming that they were close enough together so that the Stokes flow region encompassed both cylinders. Their method for determining the lift and drag forces,

however, was only accurate up to terms of order $O((\log \text{Re})^{-2})$.

In the second limit, we cannot lump the array of cylinders together. This makes the "unlumped-body" problem analogous to the multi-body convective heat transfer problem of Titcombe & Ward [18], which included the effect of long range interaction of the bodies. Each of the $N$ cylinders in the array would have its own body-shape dependent parameter $d_i$ associated with it, for $i = 1, \ldots, N$. To treat the multi-body problem, it would be necessary to formulate the related problem of the hybrid method in terms of the velocity and pressure, instead of the stream function formulation that was possible in the one-cylinder case. As in Greengard *et al.* [4], we could extend the numerical method in Section 5.1 to compute **M** from the solution to Stokes flow in a multiply connected region.

## Acknowledgement

## References

[1] J. Carrier, L. Greengard, and V. Rokhlin. A fast adaptive multipole algorithm for particle simulations. *SIAM Journal on Scientific and Statistical Computing*, 9(4):669–686, 1988.

[2] W. Chester. The matching condition for two-dimensional flow at low Reynolds number: with application to the motion of an elliptic cylinder. *Proceedings of the Royal Society of London, Series A*, 437:195–198, 1992.

[3] L. Greengard. *The Rapid Evaluation of Potential Fields in Particle Systems*. PhD thesis, MIT Press, Cambridge, 1988. ACM Distinguished Dissertations.

[4] L. Greengard, M. C. Kropinski, and A. Mayo. Integral equation methods for Stokes flow and isotropic elasticity in the plane. *Journal of Computational Physics*, 125(2):403–414, 1996.

[5] L. Greengard and V. Rokhlin. A fast algorithm for particle simulations. *Journal of Computational Physics*, 73(2):325–348, 1987.

[6] G. Hsiao and R. C. MacCamy. Solution of boundary value problems by integral equations of the first kind. *SIAM Review*, 15(4):687–705, 1973.

[7] I. Imai. On the asymptotic behaviour of viscous fluid flow at a great distance from a cylindrical body, with special reference to Filon's paradox. *Proceedings of the Royal Society*, 208:487–516, 1951.

[8] S. Kaplun. Low Reynolds number flow past a circular cylinder. *Journal of Mathematics and Mechanics*, 6(5):595–603, 1957.

[9] J. B. Keller and M. J. Ward. Asymptotics beyond all orders for a low Reynolds number flow. *Journal of Engineering Mathematics*, 30:253–265, 1996.

[10] M. C. Kropinski, M. J. Ward, and J. B. Keller. A hybrid asymptotic-numerical method for calculating low Reynolds number flows past symmetric cylindrical bodies. *SIAM Journal of Applied Mathematics*, 55:1484–1510, 1995.

[11] S. H. Lee and L. G. Leal. Low-Reynolds-number flow past cylindrical bodies of arbitrary cross-sectional shape. *Journal of Fluid Mechanics*, 164:401–427, 1986.

[12] S. J. Lighthill. *Mathematical Biofluiddynamics*. Regional conference series in applied mathematics. SIAM, Philadelphia, 1975.

[13] S. Mikhlin. *Integral Equations and their applications to certain problems in mechanics, mathematical physics and technology*. Pergammon Press, London, 1957. Translated from the Russian by A. H. Armstrong.

[14] S. G. Muskhelishvili. *Some Basic Problems of the Mathematical Theory of Elasticity*. P. Noordhoff Ltd, 1953. Translated by J. R. M. Radok.

[15] V. Z. Parton and P. I. Perlin. *Integral Equations in Elasticity*. Mir Publishers, 1982.

[16] I. Proudman and J. R. A. Pearson. Expansions at small Reynolds numbers for the flow past a sphere and a circular cylinder. *Journal of Fluid Mechanics*, 2:237–262, 1957.

[17] K. Shintani, A. Umemura, and A. Takano. Low-Reynolds-number flow past an elliptic cylinder. *Journal of Fluid Mechanics*, 136:277–289, 1983.

[18] M. S. Titcombe and M. J. Ward. Convective heat transfer past small cylindrical bodies. *Studies in Applied Mathematics*, 91:81–105, 1997.

[19] M. Van Dyke. *Perturbation Methods in Fluid Mechanics*. Parabolic Press, Stanford, 1975.

# A    Calculating the Lift Coefficient $C_L$

Imai [7] gives an expression for the drag force and lift force in terms of an arbitrary closed contour of radius $r$ surrounding the cylindrical body. Converting this expression to polar coordinates and defining the Reynolds number as

$$\varepsilon = \text{Re} \equiv \frac{\rho U_\infty L}{\mu}, \tag{A.1}$$

we can express the lift coefficient, $C_L$, and the drag coefficient, $C_D$, as

$$C_L = \frac{r}{2} \int_0^{2\pi} \left[ \sin\theta \left( \frac{\partial\psi}{\partial r} \right)^2 - \frac{\sin\theta}{r^2} \left( \frac{\partial\psi}{\partial\theta} \right)^2 + \frac{2\cos\theta}{r} \frac{\partial\psi}{\partial r} \frac{\partial\psi}{\partial\theta} \right] d\theta$$

$$+ r \int_0^{2\pi} \omega\cos\theta \frac{\partial\psi}{\partial\theta} d\theta - \frac{r^2}{\varepsilon} \int_0^{2\pi} \cos\theta \frac{\partial\omega}{\partial r} d\theta + \frac{r}{\varepsilon} \int_0^{2\pi} \omega\cos\theta \, d\theta. \quad \text{(A.2)}$$

and

$$C_D = \frac{r}{2} \int_0^{2\pi} \left[ \cos\theta \left( \frac{\partial\psi}{\partial r} \right)^2 - \frac{\cos\theta}{r^2} \left( \frac{\partial\psi}{\partial\theta} \right)^2 - \frac{2\sin\theta}{r} \frac{\partial\psi}{\partial r} \frac{\partial\psi}{\partial\theta} \right] d\theta$$

$$- r \int_0^{2\pi} \omega\sin\theta \frac{\partial\psi}{\partial\theta} d\theta + \frac{r^2}{\varepsilon} \int_0^{2\pi} \sin\theta \frac{\partial\omega}{\partial r} d\theta - \frac{r}{\varepsilon} \int_0^{2\pi} \omega\sin\theta \, d\theta. \quad \text{(A.3)}$$

Here, $\psi$ satisfies (1.2) and the vorticity $\omega$ is $\omega = -\Delta\psi$. We obtain the result (3.4), valid for $\varepsilon \to 0$ and for an arbitrarily shaped body, by evaluating (A.2) and (A.3) on a large circle (eg. $r = r_0 \gg 1$), and by using (4.2) and (4.3).

# B   Determining Matrix $M$ for an Ellipse

Figure 7(a)) shows a uniform free-stream in the positive $x$-direction about an elliptic cylinder (with major semi-axis $a$ and minor semi-axis $b$, where $a > b$) at an angle $\alpha$ to the free-stream. Figure 7(b) displays the cylinder in a new $(u, v)$ reference frame, rotated by a


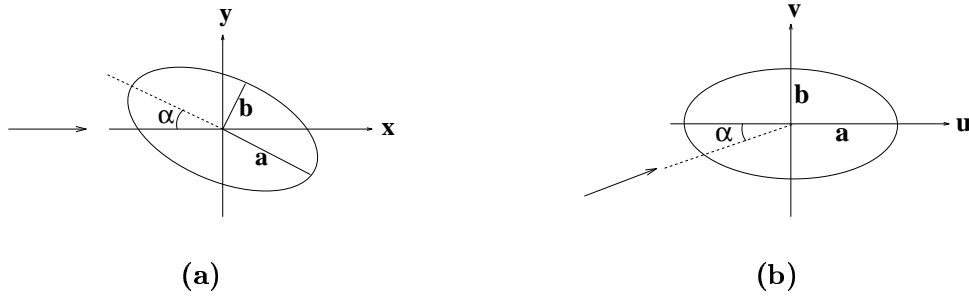
(a)                                                    (b)

Figure 7: (a) Inclined ellipse in the $(x, y)$ reference frame, with polar coordinates $x = r\cos\theta$, $y = r\sin\theta$. (b) Ellipse in the $(u, v)$ reference frame, with polar coordinates $u = r\cos\phi$, $v = r\sin\phi$.

positive angle $\alpha$ from the $(x, y)$ reference frame.

We first convert $(u, v)$ to elliptic coordinates $(\xi, \eta)$ using $u = c\cosh\xi\cos\eta$ and $v = c\sinh\xi\sin\eta$, where $c = (a^2 - b^2)^{1/2}$. Then we solve (2.2) with $D_0$ as an ellipse. To determine the matrix $\mathbf{M}$, we compare the far-field form of this solution in terms of polar coordinates,

as $r \to \infty$, with (2.3), and obtain

$$m_{11} = \frac{(b-a)\cos^2 \alpha - b}{a+b} - \log\left(\frac{a+b}{2}\right), \tag{B.1a}$$

$$m_{12} = m_{21} = \frac{(a-b)\sin \alpha \cos \alpha}{a+b}, \tag{B.1b}$$

$$m_{22} = \frac{(a-b)\cos^2 \alpha - a}{a+b} - \log\left(\frac{a+b}{2}\right). \tag{B.1c}$$

Here, $m_{ij}$ is the $ij$-th entry of the matrix $\mathbf{M}$. From (B.1), we see that for any angle of incline $\alpha$, the matrix $\mathbf{M}$ for an ellipse is symmetric. For $\alpha = 0$ (no angle of incline), $\mathbf{M}$ is diagonal and the $m_{22}$ entry must be equal to $-\log(de^{1/2})$, where $d$ is the shape-dependent parameter of the symmetric case, from Kropinski $et$ $al.$ [10], given by

$$d = \frac{a+b}{2}\exp\left(\frac{b-a}{2(a+b)}\right). \tag{B.2}$$

For no angle of incline ($\alpha = 0$),

$$m_{22} = -\log\left(\frac{a+b}{2}\right) - \frac{b}{a+b}. \tag{B.3}$$

Indeed, this expression corresponds to $-\log(de^{1/2})$ from the symmetric case.

## C   Linearized Oseen Solution, $\Psi_{oc}$, and its Derivatives

To obtain the solution, $\Psi_{oc}$, to (5.6) we first define the negative vorticity $\omega_{oc} = \Delta\Psi_{oc}$, and let $\omega_{oc}$ be of the form $\omega_{oc} = e^{\frac{1}{2}\rho\cos\theta}B_n R_c(\rho)\cos n\theta$, where $R_c(\rho)$ satisfies the modified Bessel equation of order $n$

$$z^2 \frac{\partial^2 R_c}{\partial z^2} + z\frac{\partial R_c}{\partial z} - (n^2 + z^2)R_c = 0, \tag{C.1}$$

where $z = \rho/2$. We choose $R_c(\rho) = K_n(z)$ to allow us the proper behaviour in the far-field. Therefore, in general

$$\omega_{oc} = e^{\frac{1}{2}\rho\cos\theta}\sum_{n=0}^{\infty} B_n K_n\left(\frac{\rho}{2}\right)\cos n\theta. \tag{C.2}$$

Using the small-$\rho$ structure from (5.6c) in the definition $\omega_{oc} = \Delta\Psi_{oc}$, we get that $\omega_{oc} \sim (2/\rho)\cos\theta$ as $\rho \to 0$.

From the asymptotic structure of $K_n(z)$ for small $z$, and that we will need to integrate $\omega_{oc}$ twice in obtaining $\Psi_{oc}$, we set $B_n = 0$ for $n > 1$ in (C.2), and obtain that

$$\Delta\Psi_{oc} = e^{\frac{1}{2}\rho\cos\theta}\left[B_0 K_0\left(\frac{\rho}{2}\right) + B_1 K_1\left(\frac{\rho}{2}\right)\cos\theta\right]. \tag{C.3}$$

22

Next, we write $\Psi_{oc}(\rho, \theta)$ in the form

$$\Psi_{oc}(\rho, \theta) = \sum_{n=1}^{\infty} y_n(\rho) \cos n\theta. \tag{C.4}$$

Here, we have started the summation at $n = 1$ since a term that is $\theta$-independent cannot satisfy $L_{os}\Psi_{oc} = 0$. From this form, we have that

$$\Delta\Psi_{oc} = \sum_{n=1}^{\infty} \left[ y_n''(\rho) + \frac{1}{\rho} y_n'(\rho) - \frac{n^2}{\rho^2} y_n(\rho) \right] \cos n\theta, \tag{C.5}$$

where $y_n(\rho)$ satisfies

$$y_n''(\rho) + \frac{1}{\rho} y_n'(\rho) - \frac{n^2}{\rho^2} y_n =$$
$$2B_0 K_0\left(\frac{\rho}{2}\right) I_n\left(\frac{\rho}{2}\right) + B_1 K_1\left(\frac{\rho}{2}\right) \left[ I_{n-1}\left(\frac{\rho}{2}\right) + I_{n+1}\left(\frac{\rho}{2}\right) \right], \qquad n > 0. \tag{C.6}$$

We let $y_n(\rho) = (\rho/n) f_n(\rho/2)$ and $z = \rho/2$, and so $f_n(z)$ satisfies

$$f_n''(z) + \frac{3}{z} f_n'(z) + \frac{1-n^2}{z^2} f_n(z) = \frac{2n}{z} \{B_1 K_1(z)[I_{n-1}(z) + I_{n+1}(z)] + 2B_0 K_0(z)\} \tag{C.7}$$

The solution to (C.7), or equivalently (C.6), determines the solution for $\Psi_{oc}$.

We follow Shintani $et$ $al.$ [17] and try $f_n(z)$ of the form

$$f_n(z) = \frac{\beta n}{z} K_0(z) I_n(z). \tag{C.8}$$

Substituting this form into (C.7), we see that we require $\beta = 2B_0$ and $\beta = -2B_1$. We accomplish this with $B_1 = 1$, $\beta = -2$ and $B_0 = -1$. Finally, we obtain that

$$\Psi_{oc}(\rho, \theta) = -4 \sum_{n=1}^{\infty} K_0\left(\frac{\rho}{2}\right) I_n\left(\frac{\rho}{2}\right) \cos n\theta. \tag{C.9}$$

Using (C.3) with $B_0 = -1$ and $B_1 = 1$, and (C.9), we obtain analytical expressions for certain derivatives of $\Psi_{oc}$, which are

$$\partial_\rho \Psi_{oc} = e^{x/2} \left[ K_1\left(\frac{\rho}{2}\right) - \cos\theta K_0\left(\frac{\rho}{2}\right) \right] + K_0\left(\frac{\rho}{2}\right) I_1\left(\frac{\rho}{2}\right) - K_1\left(\frac{\rho}{2}\right) I_0\left(\frac{\rho}{2}\right), \tag{C.10a}$$

$$\partial_\theta \Psi_{oc} = e^{x/2} K_0\left(\frac{\rho}{2}\right) \rho \sin\theta, \tag{C.10b}$$

$$2\partial_\rho \Delta\Psi_{oc} = e^{x/2} \left[ -2K_0\left(\frac{\rho}{2}\right) \cos\theta + K_1\left(\frac{\rho}{2}\right) \cos^2\theta + K_1\left(\frac{\rho}{2}\right) - \frac{2}{\rho} K_1\left(\frac{\rho}{2}\right) \cos\theta \right], \tag{C.10c}$$

$$2\partial_\theta \Delta\Psi_{oc} = -e^{x/2} \sin\theta \left[ -\rho K_0\left(\frac{\rho}{2}\right) + \rho K_1\left(\frac{\rho}{2}\right) \cos\theta + 2K_1\left(\frac{\rho}{2}\right) \right]. \tag{C.10d}$$

Here, $x = \rho \cos \theta$. The corresponding analytical formulae for various derivatives of $\Psi_{0s}$, from Kropinski *et al.* [10], are

$$\partial_\rho \Psi_{os} = -e^{x/2} K_0 \left( \frac{\rho}{2} \right) \sin \theta, \tag{C.11a}$$

$$\partial_\theta \Psi_{os} = -\rho e^{x/2} \left[ K_1 \left( \frac{\rho}{2} \right) + K_0 \left( \frac{\rho}{2} \right) \cos \theta \right] + 2, \tag{C.11b}$$

$$2 \partial_\rho \Delta \Psi_{os} = e^{x/2} \sin \theta \left[ K_1 \left( \frac{\rho}{2} \right) \cos \theta - K_0 \left( \frac{\rho}{2} \right) - \frac{2}{\rho} K_1 \left( \frac{\rho}{2} \right) \right], \tag{C.11c}$$

$$2 \partial_\theta \Delta \Psi_{os} = e^{x/2} K_1 \left( \frac{\rho}{2} \right) [2 \cos \theta - \rho \sin^2 \theta]. \tag{C.11d}$$

Again, $x = \rho \cos \theta$. We require these expressions in numerically evaluating the Jacobian, $J_\rho$, in (5.11a).